

Large-area, Highly Uniform Evaporated Formamidinium Lead Triiodide Thin-films for Solar Cells

Juliane Borchert, Rebecca L. Milot, Jay B. Patel, Christopher L. Davies, Adam
D. Wright, Laura Martínez Maestro, Henry J. Snaith, Laura M. Herz, and
Michael B. Johnston*

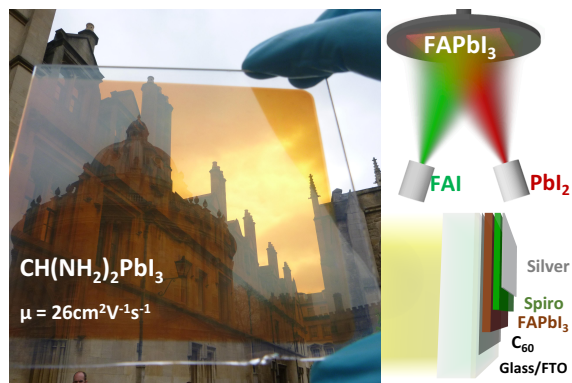
*Clarendon Laboratory, Department of Physics, University of Oxford, Parks Road,
OX1 3PU, United Kingdom*

E-mail: michael.johnston@physics.ox.ac.uk

Abstract

Perovskite thin-film solar cells are one of the most promising emerging renewable energy technologies because of their potential for low-cost, large-area fabrication combined with high energy conversion efficiencies. Recently, formamidinium lead triiodide (FAPbI₃) and other formamidinium (CH(NH₂)₂) based perovskites have been explored as interesting alternatives to methylammonium lead triiodide (MAPbI₃), because they exhibit better thermal stability. However at present a major challenge is up-scaling of perovskite solar cells from small test-cells to full solar modules. We show that co-evaporation is a scalable method for the deposition of homogeneous FAPbI₃ thin-films over large areas. The method allows precise control over film thickness and results in highly uniform, pin-hole free layers. Our films exhibited a high charge-carrier mobility of 26 cm²V⁻¹s⁻¹, excellent optical properties and a bimolecular recombination constant

of $7 \times 10^{-11} \text{ cm}^3 \text{ s}^{-1}$. Solar cells fabricated using these vapor-deposited layers within a regular device architecture produced stabilized power conversion efficiencies of up to 14.2 %. Thus we demonstrate that efficient FAPbI₃ solar cells can be vapor-deposited, which opens up a pathway towards large-area stable perovskite photovoltaics.



Hybrid organic–inorganic perovskite halide solar cells have attracted much attention in recent years because of their remarkably fast rise in power conversion efficiencies (PCE).¹ While PCEs above 20 % have been achieved by multiple research groups,^{2–4} the stability and up-scalability of perovskite solar cells remain obstacles to their commercialization. Methylammonium lead triiodide ($\text{CH}_3\text{NH}_3\text{PbI}_3 = \text{MAPbI}_3$) has been the most commonly used and investigated perovskite solar cell material. However more recently formamidinium lead triiodide ($\text{CH}(\text{NH}_2)_2\text{PbI}_3 = \text{FAPbI}_3$) and other perovskites containing formamidinium have been studied as they offer a number of advantages over MAPbI_3 . Specifically, FAPbI_3 has a narrower band gap of 1.47 eV which results in an extension of the absorption into the near infrared,⁵ and FAPbI_3 also exhibits better thermal stability than MAPbI_3 .⁶ Mixed-cation perovskites combining formamidinium and other cations such as methylammonium or cesium have been shown to be even more thermally stable,^{7,8} while using both mixed cations and mixed halides enables stable perovskite thin films to be created with a widely tunable band gap.⁹

FAPbI_3 thin-films have been fabricated using a variety of methods, with spin-coating from solution being the most common.^{6,10} Others have used pre-deposited PbI_2 films which they converted into FAPbI_3 by dipping in solutions containing FAI ,⁵ and it has also been demonstrated that FAPbI_3 thin-films can be grown in a chemical vapor deposition (CVD) furnace.¹¹

Vacuum based deposition processes such as co-evaporation are advantageous because they result in highly uniform, pin-hole free, smooth thin films.¹² Pin-hole free films are particularly important for large-area solar cells in order to avoid short circuits between electron and hole transport layers that limit PCEs and fill factors. Good thickness uniformity and low roughness is important for reliable solar cell production and also facilitates advanced optoelectronic characterization of the material.¹² Using co-evaporation and highly optimized contact layers efficiencies of up to 20% have been reached for MAPbI_3 based solar cells.³ Additionally, vacuum based deposition does not require solvents, so is a ideal method for

depositing perovskite thin films in multi-layer stacks and on sensitive substrates. This is particularly useful for the fabrication of tandem solar cells^{8,13} and solar cells on flexible substrates.

In this study, we combine the advantages of formamidinium based perovskites with the advantages of thermal evaporation under vacuum. We used co-evaporation to deposit large area ($8\text{ cm} \times 8\text{ cm}$), highly uniform FAPbI_3 thin-films that possessed excellent material properties. The films exhibited a high charge carrier mobility of $26\text{ cm}^2\text{V}^{-1}\text{s}^{-1}$ and a very low surface roughness with a root mean square (R_{RMS}) of only 6.2 nm . We also fabricated efficient solar cell devices based on co-evaporated FAPbI_3 which produced PCEs of up to 15.8% , with a stabilised power output (SPO) efficiency of 14.2% .

Solar cells were fabricated using a simple planar architecture on fluoride-doped tin oxide (FTO) coated glass substrates. Briefly, they consisted of an evaporated C_{60} layer as the electron transport layer,¹⁴ a 300 nm thick absorber layer of co-evaporated FAPbI_3 and a spin-coated hole transport layer of 2,2',7,7'-Tetrakis-(*N*, *N*-di-4-methoxyphenylamino)-9,9'-spirobifluorene (Spiro-OMeTAD). Finally, multiple 100 nm thick silver electrodes with an area of 9.19 mm^2 were evaporated, these electrodes defined the pixel size of the test solar cell devices. Full details of device fabrication are provided in the Supporting Information. The device performance was assessed using current density–voltage (J–V) sweeps and photocurrent spectroscopy under simulated sunlight. As shown in Figure 1a the power conversion efficiency (PCE) of our champion cell was 15.8% with an open circuit voltage (V_{OC}) of 1.01 V and a short circuit current (J_{SC}) of 22.1 mAcm^{-2} . To test the stabilisation of the solar cell performance under working conditions, the same cell was held close to the maximum power point for 50 s . The PCE stabilized at 14.2% (Figure 1b) and the current stabilized at 17 mAcm^{-2} .

Figure 1c shows the external quantum efficiency (EQE) spectrum of the champion device measured in short circuit under 1 sun (1 kW/cm^2 AM1.5) illumination. The EQE peaks at 80% and shows high values over the wavelength range $400\text{ nm} - 600\text{ nm}$. However a drop

in EQE to values $\sim 60\%$ is observed for wavelengths between 600 nm and the FAPbI₃ band-edge. We attribute this feature to optical interference in the planar device-stack, coupled with a lower absorption coefficient of the perovskite layer at longer wavelengths. We therefore anticipate that producing devices with a thicker FAPbI₃ layer, and utilizing optical modelling to optimize the thicknesses of all layers in the device stack would further improve the PCE of these cells.

The integrated current over the spectrum is 19 mAcm^{-2} which is close to the J_{SC} recorded in the J–V measurements: 22 mAcm^{-2} for both the forward and reverse scan, and 17 mAcm^{-2} stabilized. Additional cell performance data can be found in the Supporting Information. Overall, we were able to fabricate solar cells with a high PCE which also stabilized at similarly high efficiencies. This result shows that vapor depositing FAPbI₃ yields efficient solar cells in a relatively simple, planar cell architecture.

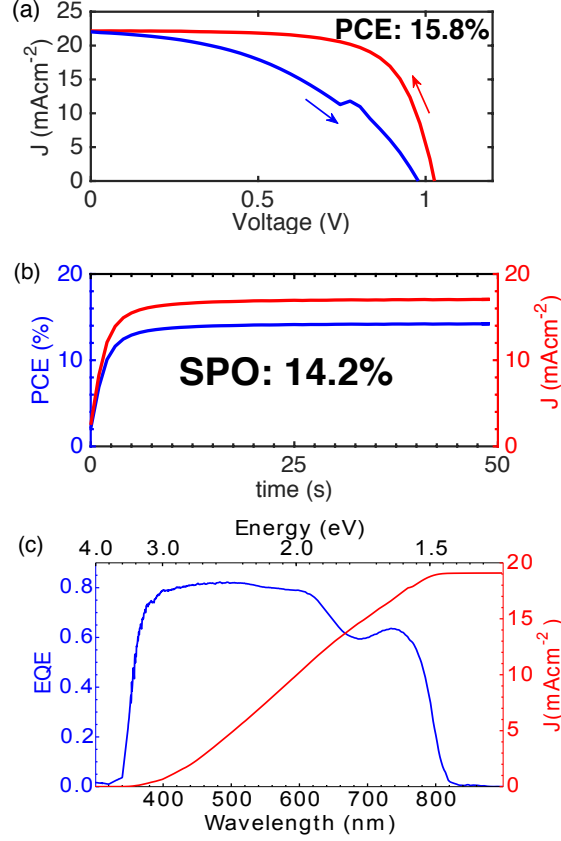


Figure 1: (a) Current–voltage (J – V) curve of the champion evaporated FAPbI₃ device. The short circuit current density (J_{SC}) was 22.1 mAcm⁻², the open circuit voltage (V_{OC}) was 1.01 V and the power conversion efficiency (PCE) was 15.8%. Significant hysteresis can be observed between the forward (blue) and reverse (red) sweeps. (b) The stabilized power output measurement (SPO), showing a stabilised efficiency of 14.2% (blue) and a stabilised current of 17 mAcm⁻² (red). (c) The external quantum efficiency (EQE) spectrum (blue) of the same device with the integrated current over the EQE spectrum (red) being 19 mAcm⁻².

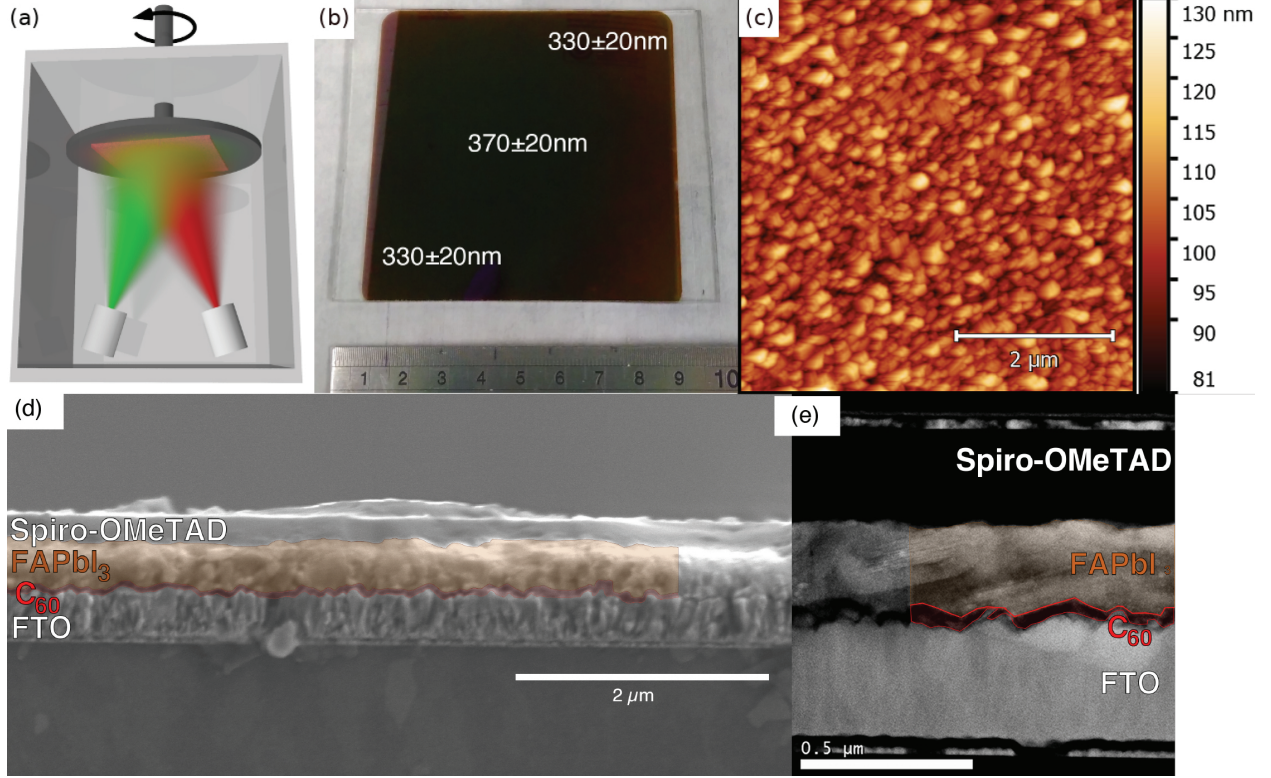


Figure 2: (a) Schematic diagram of the dual-source co-evaporation system used in this study. (b) Photograph of a $8\text{ cm} \times 8\text{ cm}$ thin film of FAPbI_3 deposited on a glass substrate. The image shows the substrate after thermal annealing at 170°C for 1 minute. The results of thickness measurements at 3 positions are superimposed on the image, and a metal ruler with a centimeter scale is shown as a size reference. (c) Atomic force micrograph of a $5\text{ }\mu\text{m} \times 5\text{ }\mu\text{m}$ region of the sample. The surface was found to be very smooth with a root mean square roughness $R_{\text{RMS}} = 6.2\text{ nm}$. (d) A scanning electron microscopy image and (e) a scanning transmission electron microscopy image of a full FAPbI_3 solar cell. From the bottom the layers are: a glass substrate, fluorine doped tin oxide (FTO) layer, thin C_{60} layer, FAPbI_3 layer a spiro-OMeTAD layer and the silver electrode.

To assess the uniformity of the co-evaporation method, we deposited a large-area (64 cm^2) FAPbI_3 film directly onto a glass sheet. Our evaporation system had a relatively short working distance of 20 cm between the thermal sources and the rotating substrate (schematically shown in Figure 2a). Therefore it is expected that any evaporated film should be thickest the centre of the substrate, with thickness reducing as a function of radius. A photograph of the deposited film after annealing is shown in Figure 2b. We measured the thickness of the FAPbI_3 layer in three areas on this film using a profilometer. In each area at least

seven measurements were performed to calculate a mean thickness value (see Figure SI 1 for further details). The film had a thickness of 370 ± 20 nm at the centre of the substrate, and as expected, the thickness dropped as a function of radius to 330 ± 20 nm in the corners of the substrate. A straightforward approach to further improving the uniformity of the films is to use a deposition system with a large working distance.

We performed atomic force microscopy (AFM) measurements to determine the surface roughness and surface coverage of the film. Figure 2c is an AFM image recorded over an area of $5 \mu\text{m} \times 5 \mu\text{m}$. The film is very smooth with a surface roughness of only $R_{\text{RMS}} = 6.2$ nm over the image area. This value is much lower than the surface roughness of FAPbI₃ thin films produced by other methods, with reported roughness values ranging from 18 nm¹⁵ to above 100 nm.¹⁶ We also found that the film was very homogeneous and had no pinholes. We conclude that evaporation leads to significantly smoother and more homogeneous films from which we would expect very little light scattering. Indeed this is confirmed by the visible absorption and transmission and reflection spectra shown in Figure 3a where there is very little scatter below the onset of absorption. The absorption onset is around 1.5 eV which is consistent with the previously reported values for the absorption onset in solution processed FAPbI₃. Together, the profilometer, AFM and absorption measurements show that we fabricated very uniform and smooth FAPbI₃ thin-films.

To clarify the crystal phases present in the thin film we performed X-ray diffraction measurements. At room temperature, FAPbI₃ can be either in a black, trigonal, perovskite phase or in a yellow, hexagonal, non-perovskite phase.^{17,18} Only thin films in the black phase are suitable for use as absorbers in solar cells so it is necessary to ensure that the film is in the right phase. The diffraction patterns are shown in Figure 3c and confirms that after 1 minute of annealing at 170° C the material was in the black perovskite α – FAPbI₃ phase. In the annealed sample, all X-ray reflections are consistent with this α structure, however in the as-deposited (unannealed) sample, the intensity of the perovskite reflection is strongly reduced, and the most intense peaks are consistent with the yellow, non-perovskite δ phase

of FAPbI₃.¹⁷ This confirms that in the as-deposited film the yellow δ – FAPbI₃ is dominant and upon annealing it is converted to the black α – FAPbI₃ phase. In evaporated MAPbI₃ thin films, annealing is not necessary to obtain high solar cell efficiencies¹⁹ because there are no competing non-perovskite MAPbI₃ phases. In contrast, for FAPbI₃ annealing is essential in order to obtain the perovskite phase. Overall, we observed the same phase behaviour as has been reported for solution processed FAPbI₃¹⁸ and single crystals.¹⁷ Interestingly for evaporated FAPbI₃ thin-films only a very short annealing is necessary to obtain the desired α -phase. It is well known that the α -FAPbI₃ phase is not long-term stable and converts to a yellow hexagonal phase when exposed to humidity (see Figure S5). To address this problem co-evaporation of cesium, methylammonium or bromide could be used to stabilize the perovskite phase.

To learn more about the morphology of the films and the crystal quality, we performed scanning electron microscopy (SEM) and scanning transmission electron microscopy (STEM) on full solar cell devices. A typical cross-sectional SEM image of a device is shown in Figure 2d where a smooth, uniform film of FAPbI₃ (colored brown in the image) can be seen. In our survey of cross-sections we did not observe any evidence of pinholes in the FAPbI₃ layer. To observe the crystal quality and interfaces, high-resolution STEM images were taken on thin cross-sectional lamella of the device. The lamella were prepared using a focused ion beam (FIB), as described in the Supporting Information. The STEM image in Figure 2e shows crystallites of different orientations within the perovskite film, with some extending vertically through the film. The STEM image also shows high contrast between the FAPbI₃ (bright) and the carbon rich (dark) C₆₀ and Spiro-OMeTAD that surround it. Close inspection of Figure 2e reveals regions of direct contact between the FAPbI₃ and FTO layers which has been shown previously to lead to hysteretic J-V curves similar to that shown in Figure 1a.¹⁹

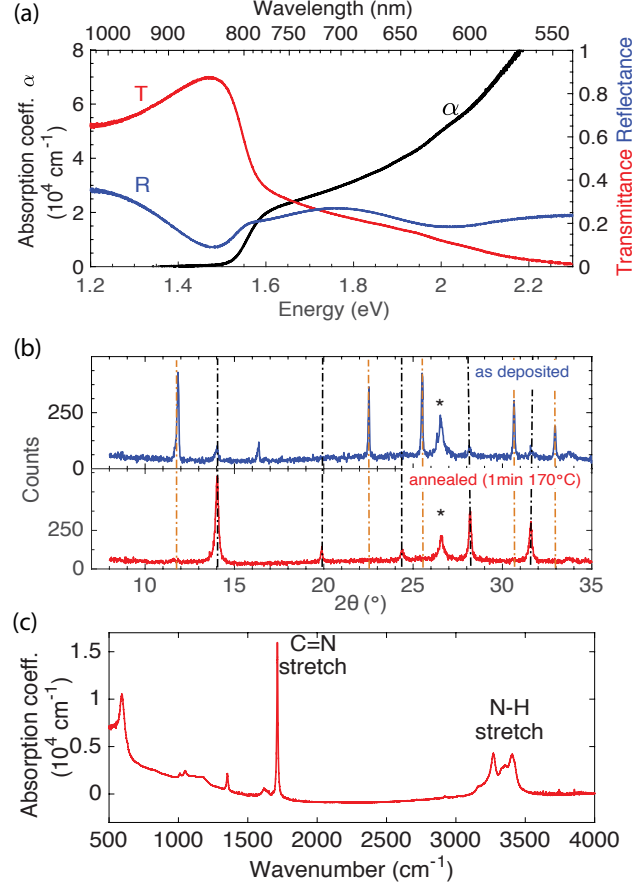


Figure 3: (a) The absorption (black line) of the co-evaporated FAPbI₃ thin-films in the visible is calculated from the transmission (red line) and reflection (blue line) spectra. As expected an absorption onset around 1.5 eV is observed. (b) The infrared absorption spectrum of the film showing the characteristic absorption peaks for FAPbI₃. (c) The X-ray diffraction pattern for an as-deposited and for an annealed film. The orange lines mark the expected position corresponding to the yellow non-perovskite δ – FAPbI₃ phase, whereas the black dashed lines mark the peaks matching the perovskite α – FAPbI₃ phase.¹⁷ The star marks the FTO substrate peak.

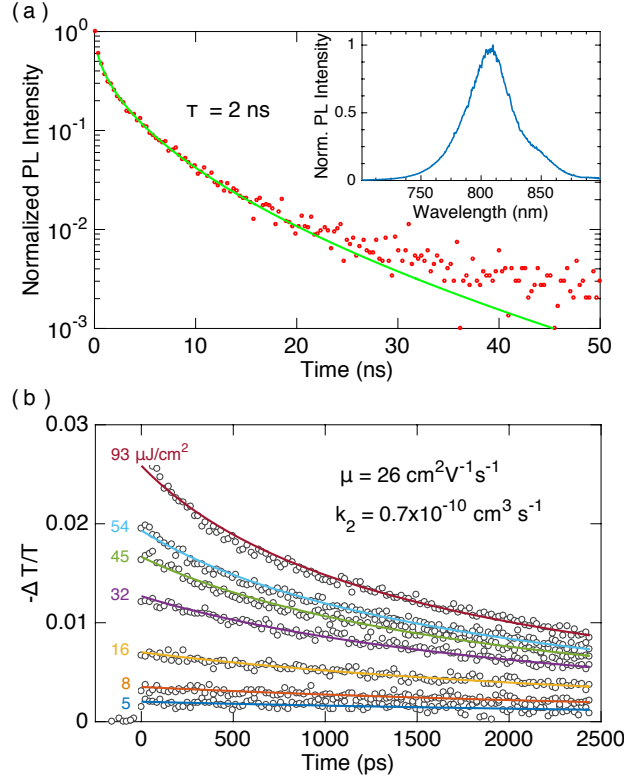


Figure 4: (a) Photoluminescence (PL) from an evaporated FAPbI₃ thin film. The PL decay is fit using a stretched exponential function to extract an average monomolecular charge-carrier lifetime of 2 ns. The PL spectrum shown in the inset has a peak at 805 nm (1.54 eV). (b) Optical pump / THz probe measurements of the charge-carrier recombination dynamics in the evaporated FAPbI₃ thin film on z-cut quartz. The sample was photoexcited at 400 nm with various fluences ranging from 5–93 $\mu\text{J}/\text{cm}^2$ as labeled on the graph. The open circles represent experimental data points, and the solid lines are fits to Equation 1 of the Supporting Information.

The photoluminescence (PL) spectrum of co-evaporated and annealed FAPbI₃ film is shown in the inset of Figure 4a. The PL peak is at a wavelength of approximately 805 nm (1.54 eV) in agreement with previous reports for solution-processed FAPbI₃.^{6,17,20} The full width at half-maximum of the PL spectrum for the vapor-deposited sample was 79 meV, which is slightly narrower than that previously reported for a solution-processed sample (88 meV).²⁰ Since PL broadening is a combination of both homogeneous broadening and disorder broadening,²¹ the narrower PL emission observed from the evaporated films may be

an indication of reduced disorder, however an in-depth study of PL as a function of excitation fluence and temperature would be required to confirm this. Figure 4a shows the measured time-resolved PL transient fitted with a stretched exponential function in order to account for a superposition of exponential decays.^{19,22} The average monomolecular lifetime τ of these decays is 2 ns, which is significantly lower than that typically reported for solution processed FAPbI₃ films.^{6,23,24} Our measured lifetimes are similar to previously reported lifetimes for vapor deposited MAPbI₃ films.²⁵ Optimisation of deposition parameters to increase the PL lifetime offers another opportunity of improving the efficiency of solar cells based on these films, which show remarkably high PCEs given the very short PL lifetimes.

THz photoconductivity measurements were performed to assess the charge mobility and recombination dynamics in co-evaporated FAPbI₃. Figure 4b shows the change in photoconductivity for a thin film of co-evaporated FAPbI₃ as a function of time after photo-excitation with 35 fs laser pulses. From these data the charge carrier mobility was found to be $26 \text{ cm}^2 \text{V}^{-1} \text{s}^{-1}$ and an apparent²⁶ bimolecular recombination rate constant of $k_2^{\text{apparent}} = 0.7 \times 10^{-10} \text{ cm}^3 \text{s}^{-1}$ was extracted. Both parameters are nearly identical to the values determined for solution-processed FAPbI₃ films.^{24,27} Using the measured carrier lifetime and mobility we extract a charge carrier diffusion length²⁴ of 360 nm for a charge-carrier density typical for this material under solar illumination (10^{15} cm^{-3}).²⁷ This is longer than the thickness of our absorber layer and therefore sufficiently long to allow the charges to migrate to the interfaces with the charge transport layers. These THz measurements show that the evaporated FAPbI₃ possesses good charge conduction properties, comparable with the perovskite materials used in high efficiency solar cells.

We were able to co-evaporate formamidinium iodide and lead iodide to deposit FAPbI₃ thin films. The deposited films were smooth and uniform over a large area of roughly 8 by 8 cm which demonstrates the advantages of vapor deposition for large-area perovskite solar cells. The film properties were similar to previously reported properties of FAPbI₃.

We fabricated solar cells from these thin films and achieved a stabilized power conversion efficiency of 14.2%. This is a highly promising result which with further improvements in interface engineering can lead to even higher efficiencies. Being able to vapor deposit FAPbI_3 is a key step towards the up-scaling of perovskite solar cells.²⁸ It opens up the possibility of fabricating the more stable, multi-cation perovskites such as $\text{FA}_y\text{Cs}_{y-1}\text{Pb}(\text{I}_{1-x}\text{Br}_x)_3$ using the highly scalable co-evaporation route. Thus our results are an important milestone on the way to large-area, stable thin-film perovskite solar cells.

Acknowledgement

The authors gratefully acknowledge the financial support from the Engineering and Physical Sciences Research Council (UK) (EPSRC). J.B.P. thanks the EPSRC and Merck Chemicals for the financial support through an Industrial CASE studentship. J.B. thanks the EPSRC for funding via the Centre for Doctoral Training in New and Sustainable Photovoltaics. A.D.W. thanks the EPSRC for funding via the Centre for Doctoral Training in Plastic Electronics.

Supporting Information Available

Additional experimental procedures and characterization data such as scanning electron microscopy images, additional atomic force microscopy images, photos illustrating the phase transition to the yellow phase and additional data about the spread of solar cell performance can be found in the Supporting Information.

References

- (1) Correa-Baena, J.-P.; Abate, A.; Saliba, M.; Tress, W.; Jacobsson, T. J.; Grätzel, M.; Hagfeldt, A. The rapid evolution of highly efficient perovskite solar cells. *Energy Environ. Sci. Energy Environ. Sci.* **2017**, *10*, 710–727.
- (2) Yang, W. S.; Park, B.-W.; Jung, E. H.; Jeon, N. J.; Kim, Y. C.; Lee, D. U.; Shin, S. S.; Seo, J.; Kim, E. K.; Noh, J. H.; Seok, S. I. Iodide management in formamidinium-lead-halide-based perovskite layers for efficient solar cells. *Science* **2017**, *356*, 1376–1379.
- (3) Momblona, C.; Gil-Escrig, L. N.; Bandiello, E.; Hutter, E. M.; Sessolo, M.; Lederer, K.; Blochwitz-Nimoth, J.; Bolink, H. J. Efficient vacuum deposited p-i-n and n-i-p perovskite solar cells employing doped charge transport layers. *Energy Environ. Sci.* **2016**, *9*, 3456–3463.
- (4) Saliba, M.; Matsui, T.; Seo, J.-Y.; Domanski, K.; Correa-Baena, J.-P.; Nazeeruddin, M. K.; Zakeeruddin, S. M.; Tress, W.; Abate, A.; Hagfeldt, A.; et al., Cesium-containing triple cation perovskite solar cells: improved stability, reproducibility and high efficiency. *Energy Environ. Sci.* **2016**, *9*, 1989–1997.
- (5) Koh, T. M.; Fu, K.; Fang, Y.; Chen, S.; Sum, T. C.; Mathews, N.; Mhaisalkar, S. G.; Boix, P. P.; Baikie, T. Formamidinium-containing metal-halide: An alternative material for near-IR absorption perovskite solar cells. *J. Phys. Chem. C* **2014**, *118*, 16458–16462.
- (6) Eperon, G. E.; Stranks, S. D.; Menelaou, C.; Johnston, M. B.; Herz, L. M.; Snaith, H. J. Formamidinium lead trihalide: a broadly tunable perovskite for efficient planar heterojunction solar cells. *Energy Environ. Sci.* **2014**, *7*, 982–988.
- (7) Habisreutinger, S. N.; Mcmeekin, D. P.; Snaith, H. J.; Nicholas, R. J. Research Update: Strategies for improving the stability of perovskite solar cells. *APL Mater.* **2016**, *4*, 091503.

- (8) McMeekin, D. P.; Sadoughi, G.; Rehman, W.; Eperon, G. E.; Saliba, M.; Hörantner, M. T.; Haghighirad, A.; Sakai, N.; Korte, L.; Rech, B.; et al., A mixed-cation lead mixed-halide perovskite absorber for tandem solar cells. *Science* **2016**, *351*, 151–155.
- (9) Wang, Z.; McMeekin, D. P.; Sakai, N.; van Reenen, S.; Wojciechowski, K.; Patel, J. B.; Johnston, M. B.; Snaith, H. J. Efficient and air-stable mixed-cation lead mixed-halide perovskite solar cells with n-doped organic electron extraction layers. *Adv. Mater.* **2017**, *29*, 1604186.
- (10) Lv, S.; Pang, S.; Zhou, Y.; Padture, N. P.; Hu, H.; Wang, L.; Zhou, X.; Zhu, H.; Zhang, L.; Huang, C.; et al., One-step solution-processed formamidinium lead trihalide ($\text{FAPbI}_{(3-x)}\text{Cl}_x$) for mesoscopic perovskite-polymer solar cells. *Phys. Chem. Chem. Phys.* **2014**, *16*, 19206.
- (11) Leyden, M. R.; Jiang, Y.; Qi, Y. Chemical vapor deposition grown formamidinium perovskite solar modules with high steady state power and thermal stability. *J. Mater. Chem. A* **2016**, *4*, 13125–13132.
- (12) Liu, M.; Johnston, M. B.; Snaith, H. J. Efficient planar heterojunction perovskite solar cells by vapour deposition. *Nature* **2013**, *501*, 395–398.
- (13) Eperon, G. E.; Leijtens, T.; Bush, K. A.; Prasanna, R.; Green, T.; Wang, J. T.-W.; McMeekin, D. P.; Volonakis, G.; Milot, R. L.; May, R.; et al., Perovskite-perovskite tandem photovoltaics with optimized band gaps. *Science (New York, N.Y.)* **2016**, *354*, 861–865.
- (14) Zhao, D.; Ke, W.; Grice, C. R.; Cimaroli, A. J.; Tan, X.; Yang, M.; Collins, R. W.; Zhang, H.; Zhu, K.; Yan, Y. Annealing-free efficient vacuum-deposited planar perovskite solar cells with evaporated fullerenes as electron-selective layers. *Nano Energy* **2016**, *19*, 88–97.

- (15) Yu, Y.; Wang, C.; Grice, C. R.; Shrestha, N.; Chen, J.; Zhao, D.; Liao, W.; Cimaroli, A. J.; Roland, P. J.; Ellingson, R. J.; et al., Improving the performance of formamidinium and cesium lead triiodide perovskite solar cells using lead thiocyanate additives. *ChemSusChem* **2016**, *9*, 3288–3297.
- (16) Xie, Z.; Sun, S.; Yan, Y.; Zhang, L.; Hou, R.; Tian, F.; Qin, G. G. Refractive index and extinction coefficient of $\text{NH}_2\text{CH}=\text{NH}_2\text{PbI}_3$ perovskite photovoltaic material. *J. Phys.: Condens. Matter* **2017**, *29*, 245702.
- (17) Stoumpos, C. C.; Malliakas, C. D.; Kanatzidis, M. G. Semiconducting tin and lead iodide perovskites with organic cations: Phase transitions, high mobilities, and near-infrared photoluminescent properties. *Inorg. Chem.* **2013**, *52*, 9019–9038.
- (18) Binek, A.; Hanusch, F. C.; Docampo, P.; Bein, T. Stabilization of the trigonal high-temperature phase of formamidinium lead iodide. *J. Phys. Chem. Lett.* **2015**, *6*, 1249–1253.
- (19) Patel, J. B.; Wong-Leung, J.; Van Reenen, S.; Sakai, N.; Wang, J. T. W.; Parrott, E. S.; Liu, M.; Snaith, H. J.; Herz, L. M.; Johnston, M. B. Influence of interface morphology on hysteresis in vapor-deposited perovskite solar cells. *Adv. Electron. Mater.* **2016**, 1600470, 1600470.
- (20) Wright, A. D.; Verdi, C.; Milot, R. L.; Eperon, G. E.; Pérez-Osorio, M. A.; Snaith, H. J.; Giustino, F.; Johnston, M. B.; Herz, L. M. Electron–phonon coupling in hybrid lead halide perovskites. *Nat. Commun.* **2016**, *7*, 11755.
- (21) Wright, A. D.; Milot, R. L.; Eperon, G. E.; Snaith, H. J.; Johnston, M. B.; Herz, L. M. Band-Tail Recombination in Hybrid Lead Iodide Perovskite. *ADVANCED FUNCTIONAL MATERIALS* **2017**, *27*.
- (22) de Quilettes, D. W.; Vorpahl, S. M.; Stranks, S. D.; Nagaoka, H.; Eperon, G. E.;

- Ziffer, M. E.; Snaith, H. J.; Ginger, D. S. Impact of microstructure on local carrier lifetime in perovskite solar cells. *Science* **2015**, *348*, 683–686.
- (23) Pellet, N.; Gao, P.; Gregori, G.; Yang, T.-Y.; Nazeeruddin, M. K.; Maier, J.; Grätzel, M. Mixed-organic-cation perovskite photovoltaics for enhanced solar-light harvesting. *Angew. Chem., Int. Ed. Engl.* **2014**, *53*, 3151–7.
- (24) Rehman, W.; Milot, R. L.; Eperon, G. E.; Wehrenfennig, C.; Boland, J. L.; Snaith, H. J.; Johnston, M. B.; Herz, L. M. Charge-carrier dynamics and mobilities in formamidinium lead mixed-halide perovskites. *Adv. Mater.* **2015**, *27*, 7938–7944.
- (25) Patel, J. B.; Milot, R. L.; Wright, A. D.; Herz, L. M.; Johnston, M. B. Formation dynamics of $\text{CH}_3\text{NH}_3\text{PbI}_3$ perovskite following two-step layer deposition. *J. Phys. Chem. Lett.* **2016**, *7*, 96–102.
- (26) Crothers, T. W.; Milot, R. L.; Patel, J. B.; Parrott, E. S.; Schlipf, J.; Müller-Buschbaum, P.; Johnston, M. B.; Herz, L. M. Photon reabsorption masks intrinsic bimolecular charge-carrier recombination in $\text{CH}_3\text{NH}_3\text{PbI}_3$ perovskite. *Nano Letters* **2017**, *17*, 5782–5789, PMID: 28792767.
- (27) Johnston, M. B.; Herz, L. M. Hybrid perovskites for photovoltaics: Charge-carrier recombination, diffusion, and radiative efficiencies. *Acc. Chem. Res.* **2016**, *49*, 146–154.
- (28) Sessolo, M.; Momblona, C.; Gil-Escrig, L.; Bolink, H. J. Photovoltaic devices employing vacuum-deposited perovskite layers. *MRS Bulletin* **2015**, *40*, 660–666.

Graphical TOC Entry

